

The role of nanoparticle shapes and deterministic aperiodicity for the design of nanoplasmonic arrays

Carlo Forestiere^{1,3}, Giovanni Miano³, Svetlana V. Boriskina¹ & Luca Dal Negro^{1,2}

¹Department of Electrical and Computer Engineering & Photonics Center, Boston University, 8 Saint Mary's Street, Boston, MA, 02215

²Division of Materials Science and Engineering, Boston University, Boston, Massachusetts 02215, USA

³Department of Electrical Engineering, Università degli Studi di Napoli Federico II, Napoli, 80125, Italy

*Corresponding author: dalnegro@bu.edu

Abstract: In this paper, we study the role of nanoparticle shape and aperiodic arrangement in the scattering and spatial localization properties of plasmonic modes in deterministic-aperiodic (DA) arrays of metal nanoparticles. By using an efficient coupled-dipole model for the study of the electromagnetic response of large arrays excited by an external field, we demonstrate that DA structures provide enhanced spatial localization of plasmonic modes and a higher density of enhanced field states with respect to their periodic counterparts. Finally, we introduce and discuss specific design rules for the engineering and optimization of field enhancement and localization in DA arrays. Our results, which we fully validated by rigorous Generalized Mie Theory (GMT) and transition matrix (T-matrix) theory, demonstrate that DA arrays provide a robust platform for the design of a variety of novel optical devices with enhanced and controllable plasmonic fields.

©2009 Optical Society of America

OCIS codes: (240.6680) Surface plasmons; (240.6695) Surface-enhanced Raman scattering; (050.6624) Subwavelength structures; (290.4020) Mie theory.

References and links

1. M. Queffelec, *Substitution dynamical systems-spectral analysis, Lecture Notes in Mathematics*, (Springer: Berlin, 1987), Vol. **1294**.
2. E. Macia, "The role of aperiodic order in science and technology," *Rep. Prog. Phys.* **69**, 397-441 (2006).
3. S. G. Williams, "Symbolic dynamics and its applications," (American Mathematical Society, Providence, RI, 2004); ISBN, 0821831577.
4. M. R. Schroeder, *Number Theory in Science and Communication*, (Springer-Verlag, 1985).
5. P. Prusinkiewicz and A. Lindenmayer, *The Algorithmic Beauty of Plants*, (Springer, New York, 1990).
6. C. Janot, *Quasicrystals: a primer*, 2nd ed. (Oxford University Press, New York, 1997).
7. M. Dulea, M. Johansson, and R. Riklund, "Localization of electrons and electromagnetic waves in a deterministic aperiodic system," *Phys. Rev. B* **45**, 105-114 (1992).
8. L. Kroon, E. Lennholm, and R. Riklund, "Localization-delocalization in aperiodic systems," *Phys. Rev. B* **66**, 094204 (2002).
9. A. Gopinath, S. V. Boriskina, N. N. Feng, B. M. Reinhard, and L. Dal Negro, "Photonic-plasmonic scattering resonances in deterministic aperiodic structures," *Nano. Lett.* **8**, 2423-2431 (2008).
10. A. Rudinger and F. Piechon, "On the multifractal spectrum of the Fibonacci chain," *J. Phys. A: Math. Gen.* **31**, 155-164 (1998).
11. L. Dal Negro, N. N. Feng, and A. Gopinath, "Electromagnetic coupling and plasmon localization in deterministic aperiodic arrays," *J. Opt. A, Pure Appl. Opt.* **10**, 064013 (2008).
12. J. M. Luck, "Cantor spectra and scaling of gap widths in deterministic aperiodic systems," *Phys. Rev. B* **39**, 5834-5849 (1989).
13. L. Dal Negro and N. Feng, "Spectral gaps and mode localization in Fibonacci chains of metal nanoparticles," *Opt. Express* **22**, 14396-14403 (2007).
14. L. Dal Negro, C. Forestiere, G. Miano, and G. Rubinacci, "Role of aperiodic order in the spectral, localization, and scaling properties of plasmon modes for the design of nanoparticle arrays," *Phys. Rev. B* **79**, 85404 (2009).
15. A. Gopinath, S. Boriskina, B. Reinhard, and L. Dal Negro, "Deterministic aperiodic arrays of metal nanoparticles for surface-enhanced Raman scattering," *Opt. Express* **17**, 3741- 3753 (2009).

16. D. W. Brandl, N. A. Mirin, and P. Nordlander, "Plasmon modes of nanosphere trimers and quadrumers," *J. Phys. Chem. B* **110**, 12302-12310 (2006).
17. E. M. Purcell and C. R. Pennypacker, "Scattering and absorption of light by nonspherical dielectric grains," *Astrophys. J.* **186**, 705-714 (1973).
18. B. T. Draine, "The discrete dipole approximation and its application to interstellar graphite dust," *Astrophys. J.* **333**, 848-872 (1988).
19. K. L. Kelly, E. Coronado, L. Zhao, and G. C. Schatz, "The optical properties of metal nanoparticles: the influence of size, shape, and dielectric environment," *J. Phys. Chem. B* **107**, 668-677 (2003).
20. L. Zhao, K. L. Kelly, and G. C. Schatz, "The extinction spectra of silver nanoparticle arrays: influence of array structure on plasmon resonance wavelength and width," *J. Phys. Chem. B* **107**, 7343-7350 (2003).
21. C. L. Haynes, A. D. McFarland, L. Zhao, R. P. Van Duyne, and G. C. Schatz, "Nanoparticle optics: the importance of radiative dipole coupling in two-dimensional nanoparticle arrays," *J. Phys. Chem. B* **107**, 7337-7342 (2003).
22. S. Zou and G. C. Schatz, "Theoretical studies of plasmon resonances in one dimensional nanoparticles chains: narrow lineshapes with tunable widths," *Nanotech.* **17**, 2813-2820 (2006)
23. Y.-L. Xu, "Electromagnetic scattering by an aggregate of spheres," *Appl. Opt.* **34**, 4573-4588 (1995).
24. T. Wriedt and A. Doicu, *Light Scattering by Systems of Particles*, (Springer, Berlin, 2006).
25. T. Wriedt, "A review of elastic light scattering theories," *Part. Part. Syst. Charact.* **15**, 67-74 (1998).
26. L. Tsang and J. Au Kong, *Scattering of Electromagnetic Waves*, (John Wiley, NY, 2001).
27. S. A. Maier, P. G. Kik, and H. A. Atwater, "Optical pulse propagation in metal nanoparticle chain waveguides: estimation of waveguide loss," *Phys. Rev. B* **67**, 205402 (2005).
28. C. F. Bohren and D. R. Huffman, *Absorption and scattering of light by small particles*, (John Wiley, 2004).
29. P. Nordlander, C. Oubre, E. Prodan, K. Li, M. I. Stockman, "Plasmon hybridization in nanoparticle dimers," *Nano. Lett.* **4**, 899-903 (2004)
30. W. Rechberger, A. Hohenau, A. Leitner, J. R. Krenn, B. Lamprecht, F. R. Aussenegg, "Optical properties of two interacting gold nanoparticles," *Opt. Comm.* **220**, 137-141 (2003)
31. V. Shalaev, *Optical properties of nanostructured random media*, (Springer-Verlag, 2002).
32. K. Li, M. I. Stockman, and D. J. Bergman, "Self-similar chain of metal nanospheres as an efficient nanolens," *Phys. Rev. Lett.* **91**, 227402 (2003).

1. Introduction

Understanding plasmonic excitations in deterministic structures without translational invariance offers a vastly unexplored potential for the creation and manipulation of sub-wavelength localized electromagnetic fields. Deterministic-aperiodic (DA) structures, which are generated by the mathematical rules of symbolic dynamics and number theory [1-5], manifest unique light localization and transport properties associated with a great structural complexity [6-8] and can be conveniently fabricated using conventional nano-lithographic techniques [9]. These structures, which are intermediate between disordered systems and periodic ones, enable a unique control and manipulation of spatially localized plasmonic states over broadband frequency and angular spectra. When fabricated using metal nanoparticles on dielectric substrates, DA structures give rise to large plasmonic gaps, as for periodic media (i.e. photonic-plasmonic crystals) and to nanoscale field localization with strong electric field enhancement (with respect to the incident wave), like disordered random media with fractal geometries. However, differently from roughened metal surfaces and random systems, which are irreproducible and lack simple design rules, DA structures are amenable to engineering and deterministic optimization. The spatial complexity of DA structures is described by the corresponding spatial Fourier spectra, which in contrast to periodic structures, densely fills the reciprocal space with multi-fractal features [6,9-11]. In this paper, we explore DA plasmonic arrays of metal nanoparticles for the design of sub-wavelength optical fields. In particular, the discussion will be focused on the scattering and field localization properties of DA arrays generated according to the Fibonacci, Thue-Morse (TM) and Rudin-Shapiro (RS) sequences, which we have recently generalized into two spatial dimensions using simple symbolic inflations [11]. These structures are the representative members of the three known classes of deterministic non-periodic systems characterized by quasi-periodic, singular-continuous and absolutely-continuous (flat) Fourier spectra, respectively [12]. Unlike random structures, the positions of nanoparticles in these DA arrays are uniquely specified by choosing the deterministic generation rule and the minimum inter-particle separation, enabling the systematic study and optimization of their plasmonic and scattering properties. We have recently explored and investigated the spectral, localization, and dispersion properties of

dipolar eigenmodes in linear and two-dimensional DA arrays of spherical nanoparticles arranged according to Fibonacci, TM, and RS sequences [11,13]. In Fibonacci and TM systems we demonstrated the presence of large spectral gaps in the pseudo-dispersion diagrams of plasmonic modes, and we clearly established the connection between the quasi-periodic geometry of Fibonacci arrays and the resulting spectral properties of their plasmonic modes [14]. Moreover, by combining electron-beam lithography (EBL), experimental dark-field scattering and Raman spectroscopy with accurate electrodynamic calculations based on the Generalized Mie Theory (GMT), we recently demonstrated broadband, distinctive scattering resonances in DA arrays of Au nanoparticles [9] as well as spatially-averaged Raman enhancement factors of the order of $\sim 10^7$ in DA arrays of Au nano-triangles [15]. However, in the field of metal plasmonic nanostructures, the study and the device applications of DA structures are still in infancy. In particular, the accurate understanding of the optical scattering and localization properties of large arrays of metal nanoparticles without translational invariance poses significant challenges to the numerical solution methods of classical electrodynamics. In this paper, we validate and utilize an efficient numerical method based on coupled-dipoles in order to study, at reduced computational costs, large DA arrays (more than thousand interacting nanoparticles) excited by an external field. In addition, we discuss specific design rules for the engineering and optimization of field enhancement and localization with respect to the array geometry and the shapes of the nanoparticles. Our results demonstrate that DA structures provide a novel and robust platform for the engineering of novel nanoplasmonics devices with enhanced plasmonic localization and enhancement distributed over larger areas compared to periodic arrays of metal nanoparticles.

2. Computational method

The near- and far-field properties of arbitrary scattering objects can be efficiently calculated using the coupled-dipole approximation (CDA), originally developed by Purcell and Pennypacker [17] and improved by Draine [18]. This method, also known as discrete dipole approach (DDA), has been widely utilized in the context of periodic arrays of metal particles [19-22] due to its fast convergence and convenient implementation. In the following, we will briefly review the main features of this method when applied to arrays of metal nanoparticles with ellipsoidal shapes. To this purpose, we introduce a rectangular coordinate system. The fundamental directions $\hat{x}, \hat{y}, \hat{z}$ are chosen to be coincident with the three principal axes of the ellipsoids. The position vectors of the centers of the ellipsoids are indicated with $\mathbf{r}_1, \mathbf{r}_2, \dots, \mathbf{r}_N$, where N denotes the nanoparticles number. We indicate with \mathbf{p}_h the electric dipole moment of the h -th particle and with \mathbf{E}_h the electric field generated at position \mathbf{r}_h by all the particles and external sources in the frequency domain. We denote with $\varepsilon = \varepsilon(\omega)$ the dielectric constant of the metal and with $V_0 = \frac{4}{3}\pi abc$ the particle volume (a, b, c are the axes of the ellipsoid along the $x, y,$ and z directions, respectively). The value of the electric field at the center of the h -th particle minus the value of the electric field generated by the h -th particle itself is given by:

$$\mathbf{E}_h = \tilde{\alpha}_0^{-1} \mathbf{p}_h \quad (1)$$

$$\tilde{\alpha}_0^{-1} = \text{diag}(\alpha_{0,a}^{-1}, \alpha_{0,b}^{-1}, \alpha_{0,c}^{-1}) = \frac{1}{V_0} \left(\frac{\tilde{\mathbf{I}}}{\varepsilon - \varepsilon_0} + \tilde{\mathbf{A}} \right) \quad (2)$$

where $\tilde{\alpha}_0$ is the polarizability dyad, $\tilde{\mathbf{A}} = \text{diag}(A_a, A_b, A_c)$ is the diagonal dyad of the depolarizing coefficients A_a, A_b, A_c whose expressions are given by the integrals:

$$A_t = \frac{abc}{2} \int_0^\infty \frac{ds}{(s+t^2) \sqrt{(s+a^2)(s+b^2)(s+c^2)}} \quad \text{with } t = a, b, c. \quad (3)$$

In order to correctly take into account the contributions of radiative damping and depolarization of the radiation across the particle surface (due to the finite ratio of particle size to wavelength) we multiply $\tilde{\alpha}_0^{-1}$ by the diagonal matrix $\tilde{\mathbf{F}} = \text{diag}(f_a, f_b, f_c)$ with elements given in Eq. (5). This choice implements the Modified Long Wavelength Approximation (MLWA) [19], which extends the validity of CDA models to particles of finite radius. In this approximation, the electronic polarizability of the particles is expressed as:

$$\tilde{\alpha}^{-1} = \tilde{\mathbf{F}} \tilde{\alpha}_0^{-1} \quad (4)$$

$$f_t = 1 - \frac{\sqrt{(-1)}}{6\pi} \frac{k^3}{\alpha_{0,t}^{-1}} - \frac{1}{4\pi t} \frac{k^2}{\alpha_{0,t}^{-1}} \quad t = a, b, c \quad (5)$$

The value of the electric field generated by the k -th particle at the center of the h -th particle can be expressed as:

$$\mathbf{E}_{h,k} = \frac{1}{4\pi\epsilon_0} \left[\frac{k^2}{r_{h,k}} \mathbf{C}_{h,k} - \tilde{\mathbf{B}}_{h,k} \left(\frac{1}{r_{h,k}^3} - \frac{\mathbf{ik}}{r_{h,k}^2} \right) \right] e^{i\mathbf{k}r_{h,k}} \mathbf{p}_k \quad (6)$$

where $\mathbf{r}_{hk} = \mathbf{r}_h - \mathbf{r}_k$ and $\hat{\mathbf{r}}_{hk} = \frac{\mathbf{r}_{hk}}{|\mathbf{r}_{hk}|}$, $\tilde{\mathbf{B}}_{h,k}$ and $\tilde{\mathbf{C}}_{h,k}$ are dyads defined as:

$$\tilde{\mathbf{B}}_{h,k} = 3\hat{\mathbf{r}}_{h,k} \hat{\mathbf{r}}_{h,k} - \tilde{\mathbf{I}} \quad (7)$$

$$\tilde{\mathbf{C}}_{h,k} = \hat{\mathbf{r}}_{h,k} \hat{\mathbf{r}}_{h,k} - \tilde{\mathbf{I}} \quad (8)$$

The field E_h is equal to the sum of the external electric field and the electric field generated by all the other particle $\sum_{k=1; k \neq h}^N E_{h,k}$. By combining Eqs. (1)-(8) we obtain a linear system of equations governing the behavior of the dipole moments $\mathbf{p}_1, \mathbf{p}_2, \dots, \mathbf{p}_N$.

$$\tilde{\alpha}^{-1} \mathbf{p}_h - \frac{1}{4\pi\epsilon_0} \sum_{k=1, k \neq h}^N \left[\frac{k^2}{r_{h,k}} \mathbf{C}_{h,k} - \tilde{\mathbf{B}}_{h,k} \left(\frac{1}{r_{h,k}^3} - \frac{\mathbf{ik}}{r_{h,k}^2} \right) \right] e^{i\mathbf{k}r_{h,k}} \mathbf{p}_k = E_{ext}(\mathbf{r}_h) \quad (9)$$

By defining the transfer dyad of the system as:

$$\tilde{\mathbf{T}}_{hk} = \begin{cases} \frac{1}{4\pi\epsilon_0} \left\{ \frac{k^2}{r_{h,k}} \tilde{\mathbf{B}}_{h,k} - \tilde{\mathbf{C}}_{h,k} \left(\frac{1}{r_{h,k}^3} - \frac{\mathbf{ik}}{r_{h,k}^2} \right) \right\} & h \neq k \\ \tilde{\alpha}^{-1} & h=k \end{cases} \quad (10)$$

we can now formulate the full scattering problem as a set of N inhomogeneous linear equations which can be solved numerically once the excitation source is known:

$$\sum_{k=1}^N \tilde{\mathbf{T}}_{hk} \mathbf{p}_k = E_{ext}(\mathbf{r}_h) \quad h=1, \dots, N \quad (11)$$

3. Model validation

We have validated the CDA model summarized above by using the Generalized Mie Theory (GMT) [23] and the transition matrix (T-matrix) theory (TM) [24,25], which are to date the most accurate and efficient semi-analytical techniques of computational electromagnetics. Both the theories provide an analytical solution to the full Maxwell's equations, including retardation effects and all the necessary multipolar scattering orders, enabling the most accurate treatment of both the near- and the far-field response of large nanoparticle arrays of arbitrary geometries. However, the applicability of the GMT method is limited to spherical particles, while the T-matrix can in principle be applied to arbitrarily shaped particles, despite its convergence is severely affected for large arrays of non-spherical particles .

In the T-matrix method, the incident and scattered fields are expanded into a series of base functions defined in terms of the outgoing spherical vector functions M_n^3 and N_n^3 [24]:

$$E^{(i)}(\mathbf{r}) = \sum_{n=1}^N D_n \left[a_n^i M_n^3(k\mathbf{r}) + b_n^i N_n^3(k\mathbf{r}) \right] \quad (12)$$

$$E^{(s)}(\mathbf{r}) = \sum_{n=1}^N D_n \left[a_n^s M_n^3(k\mathbf{r}) + b_n^s N_n^3(k\mathbf{r}) \right] \quad (13)$$

The expansion coefficients of the scattered field $\begin{bmatrix} a^s & b^s \end{bmatrix}^T$ are related to the coefficients of the incident field $\begin{bmatrix} a^i & b^i \end{bmatrix}^T$ by the T-matrix (transition matrix) of the system:

$$\begin{bmatrix} a^s \\ b^s \end{bmatrix} = -\bar{T} \begin{bmatrix} a^i \\ b^i \end{bmatrix} \quad (14)$$

The standard scheme for computing the elements of the T-matrix relies on the null-field method [26]. For a homogeneous particle, the transition matrix is given by [24]:

$$\mathbf{T} = -\mathbf{Q}^{11}(k_s, k_i) \left[\mathbf{Q}^{31}(k_s, k_i) \right]^{-1}, \quad (15)$$

where the matrices \mathbf{Q}^{31} and \mathbf{Q}^{11} can be evaluated from the extinction theorem and the Huygens principle, respectively. These matrices can be expressed as surface integrals over the scattering objects [24]. The T-matrix method can be applied to non-spherical particles, but the scattering fields can only be calculated outside the sphere with the smallest radius subtending the whole scattering object, not necessarily connected. Because of this restriction, the applicability of the T-matrix approach is effectively limited to the calculation of the scattered fields in the far-field region, while the information on the plasmonic near-fields remains inaccessible. Given these limitations, we have validated our CDA model for the near- and far-field regions separately. We utilized the GMT approach for the calculation of the wavelength-dependent near-field spectra normalized to the incident one (field enhancement spectra) considering arrays of nanospheres, and the T-matrix for the calculation of the far-field scattering efficiencies of arrays with particles of non-spherical shapes (oblate and prolate ellipsoids).

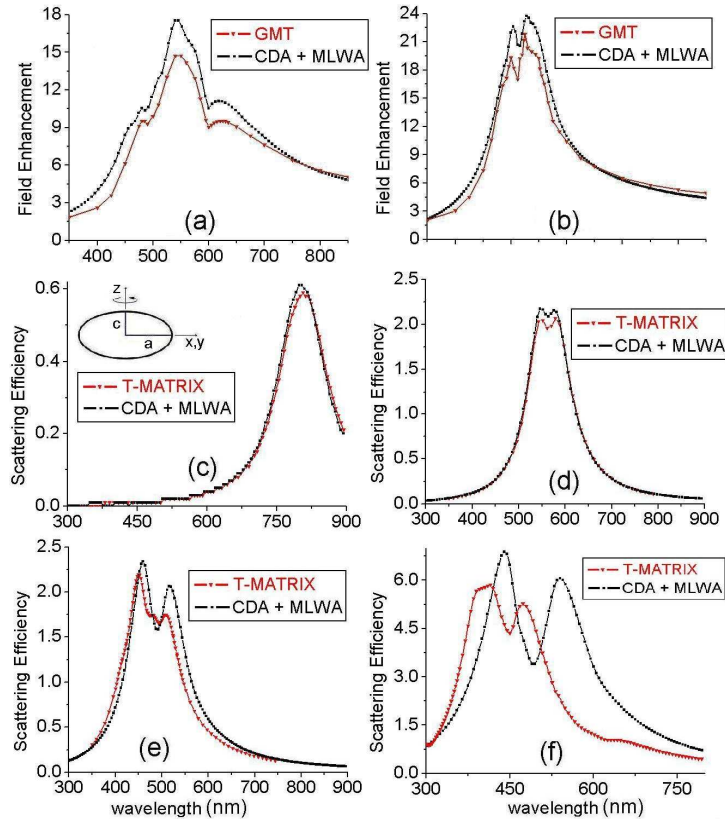


Fig. 1. Comparison of the field enhancement spectra calculated with CDA and GMT code (a-b) for a) 81-nanospheres periodic array and b) 80-nanospheres Fibonacci array. Comparison of the scattering efficiency calculated with the CDA and the T-matrix method (c-f) for Fibonacci array of 80 oblate nano-spheroids with (c) $c/a = 0.2$, and (d) $c/a=0.6$, and for Fibonacci array of 80 prolate nanoparticles with (e) $c/a = 1.5$ and (f) $c/a = 3$.

The scattering efficiency of the arrays is defined as the ratio of the scattering cross sections with the sum over the array of the geometrical cross sections of the individual particles. For the validation, we considered a periodic (square lattice) and a quasi-periodic Fibonacci array of 80 Au nanoparticles. The minimum interparticle separation (edge-to-edge) between the nanoparticles was fixed at 25 nm, irrespective of the particles shape factor defined by the ratio c/a . The radii of the spherical particles are equal to 25nm and for ellipsoidal ones we choose oblate particles with $a=b=25\text{nm}$ and $c/a=0.2, 0.6$ and prolate ones with $a=b=25\text{nm}$ and $c/a=1.5, 3$. We also notice that, based on accurate comparison with GMT the numerical calculations, particle sizes up to 75 nm in radius can be adequately described within the proposed approach. For simplicity, the Au dielectric function was modeled using a Drude model with parameters given in Ref. 27. We notice that this choice results in an underestimation of the absorptive losses of Au at short wavelengths. However, this does not affect the conclusions of our general analysis and the validity of our model, which can be flexibly adapted to the specific experimental demands. Figure 1 shows the CDA results compared to GMT and T-matrix calculations. The comparisons of the CDA and GMT calculated wavelength spectra of the local field enhancement for periodic and Fibonacci arrays of Au nanospheres are shown in Figs. 1(a) and 1(b), respectively. The scattering efficiencies of Fibonacci arrays of oblate and prolate ellipsoids calculated with CDA and T-matrix are shown in Figs. 1(c)-1(f), respectively. All the arrays have been homogeneously illuminated by an x -polarized plane wave at normal incidence. The results shown in Fig. 1

demonstrate the validity limits of the CDA calculation approach which slightly overestimates the plasmonic local fields and the scattering efficiencies in all cases except when considering particles with large shape factors ($c/a=3$). Since within the CDA approach each particle is approximated with only one dipole, discrepancies at large shape factors are expected due to the absence of multipolar scattering orders. However, we notice that the main features of the spectra calculated using the two semi-analytical approaches are also clearly present in the corresponding CDA results, which were obtained at significantly reduced computational cost, and can be utilized to investigate much larger arrays. This motivates our choice to explore the optical properties of large (thousands of interacting particles) DA arrays of metal nanoparticles within the simple and cost-effective CDA method, as we will discuss in the next sections.

4. Results and discussion.

In this section, we apply our CDA model to the understanding of the far-field and near-field plasmonic properties of periodic and DA arrays of different morphologies and nanoparticles shapes. All the particles in the arrays were modeled as rotationally symmetric ellipsoids ($a=b=25\text{nm}$) with the symmetry axis along the z direction, orthogonal to the plane of the arrays.

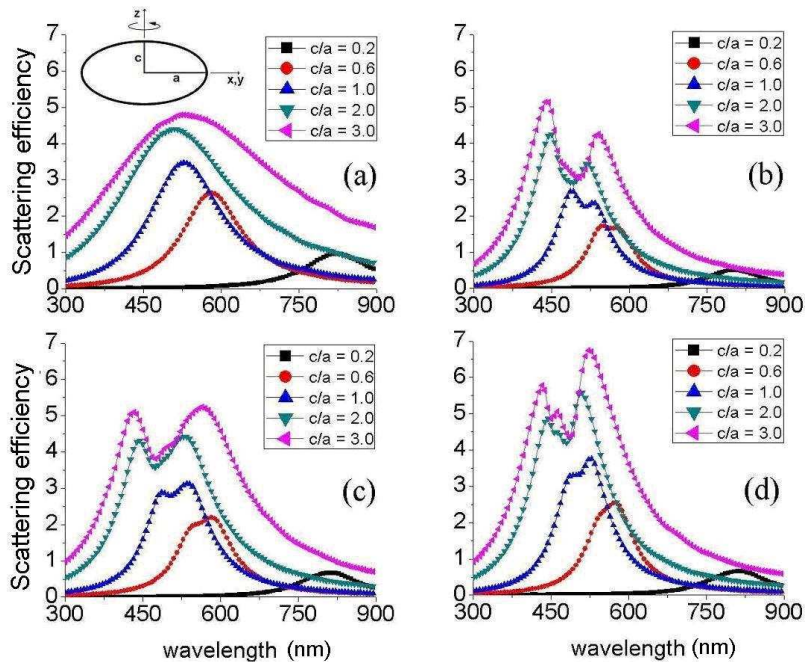


Fig. 2. Scattering efficiency versus wavelength for several values of the particles shape factor c/a and for (a) 1936 nanoparticles periodic array (b) 1428 nanoparticles Fibonacci array (c) 2048 nanoparticles Rudin Shapiro array (d) 2016 nanoparticles Thue-Morse array.

The shape factor of the ellipsoidal particles was parameterized by the c/a ratio. Oblate ellipsoids correspond to the $c/a < 1$ case (pancake shaped), spherical particles to $c/a = 1$, and prolate ellipsoids to $c/a > 1$ (cigar shaped). The minimum edge-to-edge interparticle separation between the nanoparticles in the different arrays was fixed at 25 nm for all the shapes, and the arrays were homogeneously excited by a plane wave at normal incidence with linear polarization lying in the plane of the arrays.

This choice of the interparticle separation describes the strong quasi-static coupling regime, which is important for many nanoplasmonics applications such as Surface Enhanced

Raman Scattering (SERS) sensing, plasmonic-enhanced broadband light emitters, absorbers and nano-detectors. However, a reduction of the interparticle separation below 25nm, which will further enhance the strength of the quasi-static coupling, would be extremely challenging to achieve using standard nano-fabrication techniques.

In Fig. 2 and in Fig. 3 we show the calculated scattering efficiency spectra (SCS) and maximum field enhancement spectra (MFE), in the plane of the arrays, for arrays of different morphologies and particles shapes. These are calculated for a periodic (a), Fibonacci (b), Rudin-Shapiro (c) and Thue-Morse (d) two-dimensional arrays of Au nanoparticles for five different values of shape factor c/a , as sketched in insets. In the rest of the paper, periodic arrays are composed of 1936 nanoparticles, Fibonacci of 1428, Rudin-Shapiro of 2048 and Thue-Morse of 2016.

The results in Fig. 2 clearly demonstrate the dramatic influence that the nanoparticles shapes (shape factor) have in determining the plasmonic resonant peaks of arrays that are strongly coupled in the (short-range) quasi-static regime. We notice that for periodic arrays (Fig. 2(a)) the peak positions of the plasmonic scattering peaks red-shift to longer wavelengths as the shape factor of the particles is reduced, correspondingly turning their shapes from elongated cigars to thin disks. This behavior is consistent with the well-known shape-dependent shift of the resonant condition of plasmonic modes in isolated metal nanoparticles [28].

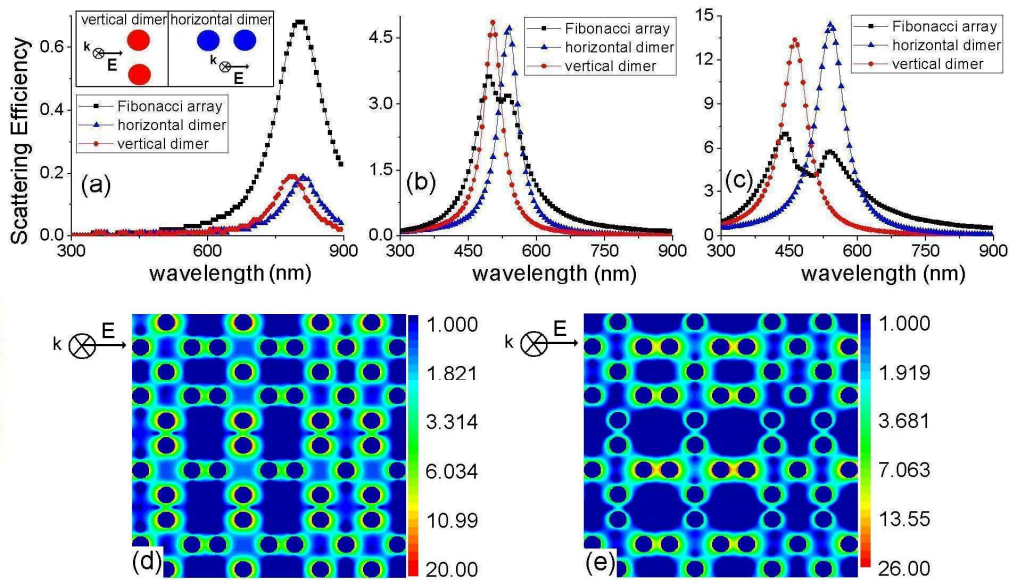


Fig. 3. Scattering efficiency versus wavelength for a 1428 nanoparticles Fibonacci structure, horizontal dimer and vertical dimer with oblate ($c/a=0.2$) (a), spherical ($c/a=1$) and prolate (c/a) shape. Electrical Field Distribution associated to the (d) blue-shifted (492nm) and (e) red-shifted (540nm) Fibonacci scattering peak of Fig. 3(b). In both cases the incoming field polarization is along the horizontal axis.

Differently from the case of periodic arrays, in DA arrays of metal nanoparticles the electromagnetic coupling results in a separation of plasmonic modes associated to the presence of an increased structural disorder. In addition, the variations in the shapes of the particles strongly affect the plasmonic field spatial distribution, which determine the in-plane electromagnetic array coupling, as we will discuss later in this paper. As shown in Figs. 2 and 4, in multi-scale DA environments, the quasi-static electromagnetic coupling is enhanced by far-field diffractive contributions, resulting in a larger plasmonic mode separation with respect to periodic structures of comparable interparticle distances [11,15].

In particular, DA arrays show the presence of two major scattering peaks, which become more predominant for prolate ellipsoids. As we will demonstrate below, these two scattering peaks, which feature a markedly different electric field distribution, are a distinctive characteristics of DA arrays associated to the simultaneous excitation of longitudinal and transverse resonant modes of different particles clusters inhomogeneously distributed across the array plane (Fig. 3). These features of DA arrays originate from the presence of multiple length scales (spatial frequencies) corresponding to a broad distribution of particle dimers (for Fibonacci and Thue-Morse) and dimers-tetramers (for Rudin-Shapiro) [9,16].

In Fig. 3(a) we compare the calculated scattering efficiency for a Fibonacci structure with oblate nanoparticles ($c/a=0.2$) with the scattering spectra of the two most recurrent cluster configurations (particle dimers) in the Fibonacci array (Fig. 3(a), inset). In Fig. 3(b) and in Fig. 3(c) we show the scattering spectra of the recurrent dimers and Fibonacci arrays with spherical and prolate ($c/a=3$) particles, respectively. Figures 3(a)-3(c) demonstrate in very clear terms that the origin of the plasmonic mode separation observed in Fig. 2 is indeed related to the simultaneous excitation of longitudinal and transverse resonances in Fibonacci arrays [29, 30].

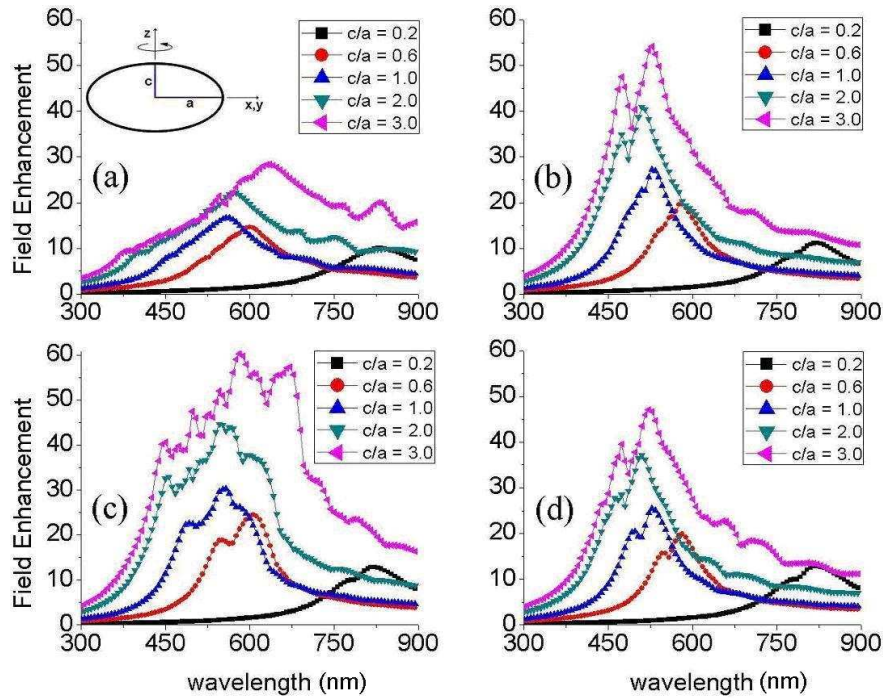


Fig. 4. Maximum field enhancement versus wavelength for several values of the ratio c/a and for (a) 1936 nanoparticles periodic array (b) 1428 nanoparticles Fibonacci array (c) 2048 nanoparticles Rudin Shapiro array (d) 2016 nanoparticles Thue-Morse array.

This is also confirmed by Fig. 3(d) and Fig. 3(e) which show the electric field patterns calculated at the two Fibonacci scattering peaks shown in Fig. 3(b). The electric field distribution associated to the blue-shifted Fibonacci scattering peak is dominated by vertically coupled dimers (Fig. 3(d)). On the opposite, longitudinally coupled dimers (Fig. 3(e)) correspond to the red-shifted scattering peak shown in Fig. 3(b). In addition, we observe in Fig. 3 that the largest plasmonic mode splitting is obtained for prolate particles due to a stronger field enhancement, which increases the dimer coupling strength. We notice that this same argument also applies to Thue-Morse and Rudin-Shapiro structures, with the exception

that more complex particle clusters (tetramers) must be taken into account resulting in more complex spectral features as shown by the near-field spectra in Fig. 4(c) and Fig. 4(d). Finally, we notice in Figs. 2 and 4 that the spectral broadening and field enhancement of DA arrays are maximized for Rudin-Shapiro arrays which are the most disordered structures characterized by continuous spatial Fourier spectra [7, 9, 11, 15].

The Field Enhancement spectra shown in Fig. 4 show very similar trends with respect to the scattering spectra discussed in Fig. 2. Moreover, we notice from Figs. 2(a) and 4(a) that the wavelength position of the peak field enhancement of periodic arrays always corresponds to well-defined dipolar modes, which are red-shifted with respect to the peak position of the scattering efficiency. This trend is particularly emphasized for periodic arrays of prolate nanoparticles. On the other hand, by comparing Figs. 2(b)-(d) and Fig. 4(b)-(d) we can notice that all the considered DA arrays behave differently. In particular, the far-field scattering and near-field enhancement spectra are almost coincident for any value of shape factor. This features are important for engineering applications. In fact, using DA arrays it is possible to roughly identify the wavelength range of maximum near-field enhancement by simple far-field scattering measurements.

The role of particles shapes in determining the strength of the electromagnetic coupling in periodic and DA arrays can be best understood by calculating the electric field profiles in the plane of the arrays. Figure 5 shows the calculated electric field distribution in the plane of a Fibonacci array consisting of (a) oblate ellipsoids ($rc = 25\text{nm}$, $c/a = 0.2$) (b) spheres ($rc = 25\text{nm}$) and (c) prolate spheroids ($rc = 25\text{nm}$ $c/a = 3$).

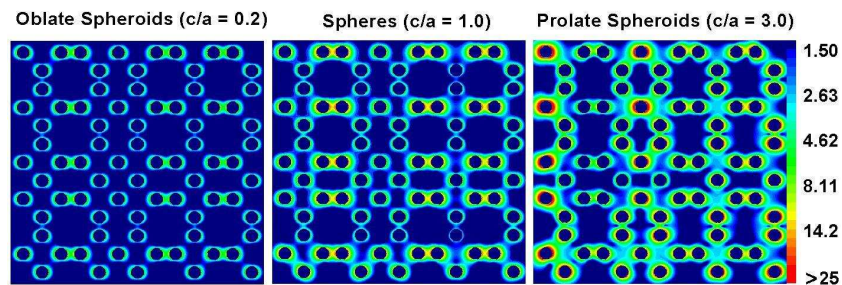


Fig. 5. Semilogarithmic plots of calculated field distribution at the wavelength of maximum field enhancement for 1428 nanoparticle Fibonacci array of (a) oblate ellipsoids ($rc = 25\text{nm}$, $c/a = 0.2$ wavelength = 822nm) (b) sphere ($rc = 25\text{nm}$ wavelength = 528nm) and (c) prolate spheroids ($rc = 25\text{nm}$ $c/a = 3$ wavelength = 474nm).

It can be observed that the in-plane electric field distribution can peak either at the nanoparticles positions or at interstitial positions between the nanoparticles, strongly affecting the in-plane electromagnetic coupling of the array. We notice from Fig. 5 that the maximum intensity of the plasmonic near-fields increases as we move from oblate to prolate ellipsoids, enhancing the electromagnetic coupling of the nanoparticles. This is expected when exciting prolate ellipsoids with an incident field polarized orthogonally to their major axis, because of the higher excitation efficiency compared to the case of prolate ellipsoids where the incident field aligns parallel to the axis. In particular, the stronger electric field intensity at interstitial nanoparticles positions is directly responsible for the observed longitudinal/transverse splitting of the plasmonic modes showed in Fig. 2 for DA arrays. The results shown in Fig. 6 fully justify this interpretation by demonstrating a direct correlation between the maximum intensity of the electric field and the wavelength separations of the two peaks observed in the scattering cross sections of the DA arrays.

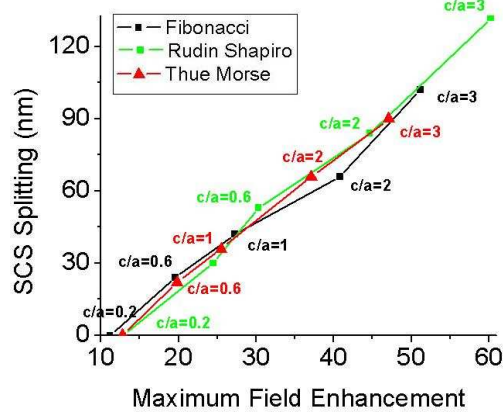


Fig. 6. Calculated wavelength splitting of the scattering cross section of DA arrays as a function of the maximum field enhancement for Thue-Morse (red triangles), Rudin-Shapiro (green squares), and Fibonacci (black squares) arrays with different nanoparticles eccentricities.

In order to discuss more quantitatively the distinctive features of the local plasmonic fields in DA arrays of nanoparticles we introduce the Cumulative Distribution Field Enhancement (CDFE) function, which measures how often a field value is represented in the plane of the arrays. This function associates to each prescribed value of field enhancement the fraction of the total area of the array in which the local field enhancement is greater than the prescribed value. Figure 7 shows the calculated CDFE function for the case of periodic, Fibonacci, Rudin-Shapiro and Thue-Morse arrays. As indicated in the Fig. 7, panel (a) corresponds to oblate ellipsoidal nanoparticles ($c/a = 0.6$), panel (b) to spherical nanoparticles ($c/a = 1$), and panel (c) to prolate ellipsoidal nanoparticles ($c/a = 2.0$)

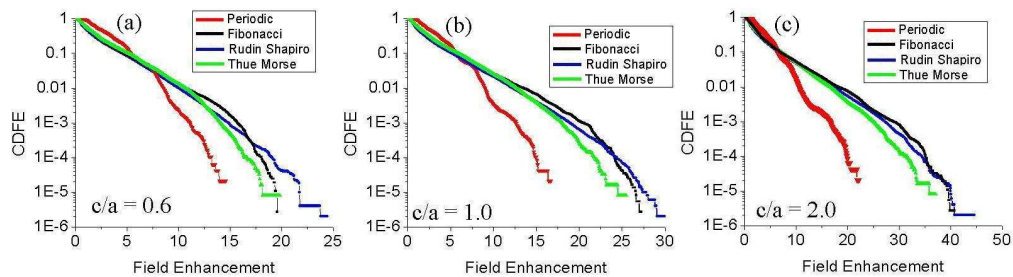


Fig. 7. Semilogarithmic plots of the CDFE function for arrays of various nanoparticle shapes (radius 25 nm) and different morphologies calculated at the wavelength of maximum field enhancement.

As a representative example, let us first discuss the case of spherical nanoparticles (panel b). We observe that all the DA arrays are characterized by higher CDFE values compared to the periodic ones. In particular, the Fibonacci CDFE is higher than the periodic case for fields greater than 5.35; this means that the fraction of the array area characterized by a field higher than 5.35 is larger than the periodic case. Moreover, for DA arrays this area becomes one order of magnitude larger than the periodic case for field values larger than 10.7. This behavior becomes even more pronounced when we consider DA arrays of prolate ellipsoidal nanoparticles. These results quantify the ability of DA arrays to provide larger values of enhanced plasmonic fields over larger areas when compared with periodic structures, which is an important feature for the engineering of device applications for active nanoplasmonics.

Another important attribute of DA arrays is their ability to confine plasmonic fields on the nanoscale. Giant field enhancement and nanoscale localization of electromagnetic fields have been thoroughly investigated in rough metal surfaces and fractal random media, both theoretically and experimentally [30,31]. These studies clearly demonstrated that the abundance of spatial frequencies and the lack of translational invariance, which characterize random and fractal systems, are key ingredients to induce resonant modes with higher spatial localization and electric field enhancement than periodic systems. However, it remains to be investigated if deterministic non-fractal plasmonic structures with multi-scale DA patterns can provide superior mode localization and field concentration with respect to their periodic counterparts.

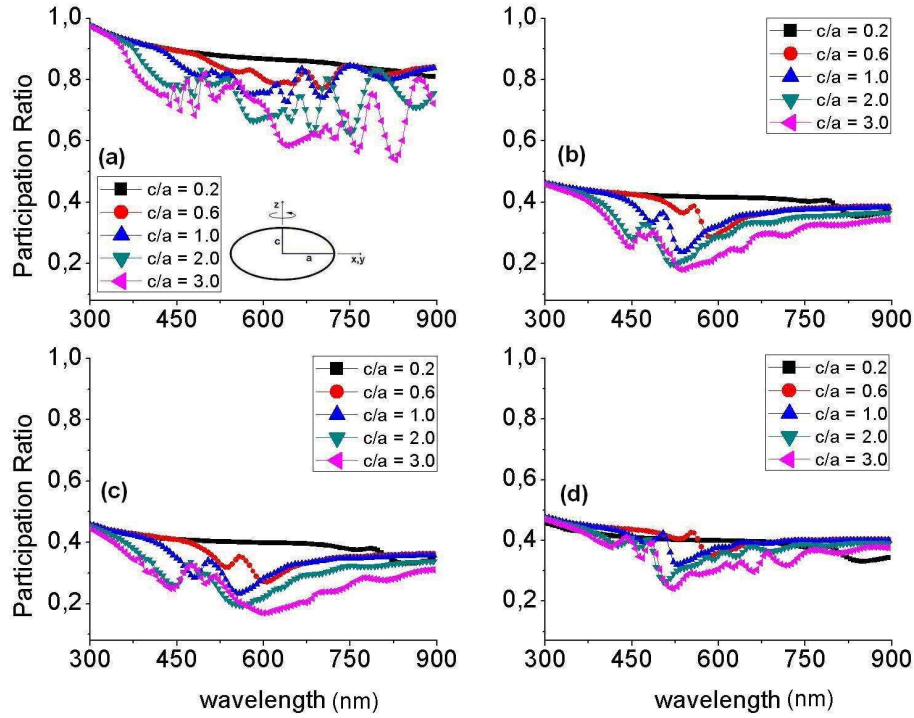


Fig. 8. Participation ratio versus wavelength for several values of the ratio c/a and for (a) 1936 nanoparticles periodic array, (b) 1428 nanoparticles Fibonacci array, (c) 2048 nanoparticles Rudin Shapiro array, and (d) 2016 nanoparticles Thue-Morse array.

In order to answer this question, we quantitatively investigate the spatial mode localization of plasmonic DA arrays by defining a localization index as the two-dimensional generalization of the participation ratio defined in Ref. 13. We define the plasmonic mode participation ratio (PR) for two-dimensional DA arrays as the following function:

$$PR = \frac{\iint_A |E(x, y)|^2}{\iint_A |E(x, y)|^4}, \quad (16)$$

where $E(x, y)$ is the electric field enhancement and the integration is performed in the $z=0$ plane of the array of area A . This definition ensures that the participation ratio for spatially localized field patterns in arrays plain is much lower than the participation ratio of spatially extended (de-localized) field patterns. Therefore, the field states with the smallest PR are the most localized ones. In Fig. 8 we show the wavelength dependence of the calculated PR, normalized to the maximum value of the periodic array, for periodic and DA arrays of

nanoparticles with different values of shape factor. As before, all the arrays share the same minimum interparticle separation of 25nm. The data in Fig. 8 demonstrate the enhanced localization of plasmonic fields in DA arrays when compared with periodic structures. In fact, we notice that DA arrays (Fig. 8(b)-8(d)) show much lower PR values with respect to periodic arrays (Fig. 8(a)) irrespective of the shape factor values and across the entire wavelength spectrum. In addition, the PR index of periodic arrays markedly fluctuates in wavelength for prolate ellipsoids, while these fluctuations are strongly reduced in DA arrays. It is also interesting to notice that while in Fibonacci (Fig. 8(b)) and Thue-Morse (Fig. 8(d)) arrays the PR spectrum is strongly peaked at a well-defined wavelength, Rudin-Shapiro arrays (Fig. 8(c)) feature a broader PR spectrum appreciably lower than all the other structures, as a result of their increased structural disorder. These results demonstrate unambiguously that the effect of increasing the “deterministic disorder” from periodic to Rudin-Shapiro structures induces a large number of strongly localized plasmonic states with progressively increasing degree of spatial localization and broader spectra. We have shown so far that DA arrays provide stronger field localization, and larger values of enhancement occurring over larger areas when compared with periodic structures. However, another important aspect for the engineering of DA arrays is the ability to identify robust optimization criteria for purpose-driven nanoplasmonics applications. This possibility is clearly missing in random structures due to their characteristic lack of reproducibility, which fundamentally limits their engineering applications.

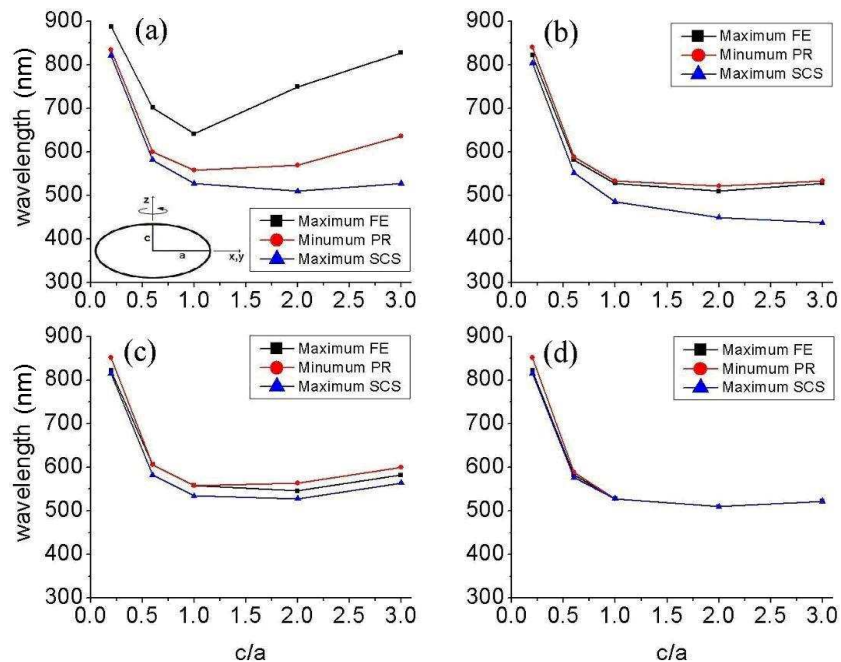


Fig. 9. Wavelength positions of the maximum field enhancement (square), maximum extinction efficiency (triangle) and minimum participation ratio (circle) versus the particles shape factor c/a for (a) 1936 nanoparticles periodic array, (b) 1428 nanoparticles Fibonacci array, (c) 2048 nanoparticles Rudin Shapiro array, and (d) 2016 nanoparticles Thue-Morse array.

In order to investigate the specific engineering design rules of DA nanoplasmonic arrays, we have plotted in Fig. 9 the wavelength positions corresponding to the maximum light scattering cross section (blue triangles), maximum electric field enhancement (black squares) and minimum PR (red circle) for different values of shape factor. We can notice that while in the case of periodic arrays (Fig. 9(a)) these three parameters are maximized at very different

wavelengths, requiring a very careful optimization for each of them separately, this is not the case for DA arrays. In fact, as shown in Figs. 9(b)-9(d), the three targeted parameters are simultaneously maximized for DA arrays. This behavior is best displayed by Thue-Morse and Rudin-Shapiro structures (Fig. 9(c) and 9(d)) due to the increased spatial disorder and reduced symmetry, which favors the simultaneous optimization of scattering, field enhancement and localization at any given frequency. This is the direct consequence of the broadband character of the plasmonic properties of DA arrays compared to periodic ones. Interestingly, we notice in periodic structures (Fig. 9(a)) a non-monotonic trend of the maximum field enhancement, scattering cross section and the minimum PR as the particles shape factor ratio c/a decreases from its maximum value. This behavior is not followed by all the DA arrays, which feature an almost monotonic shift to longer wavelengths (red-shift) as the particles shape factor is reduced from the maximum value. These results are explained by the tuning of the in-plane electromagnetic coupling induced by the variations in the particles shape factor, as discussed in relation to Fig. 5. The results shown in Fig. 9 give us a simple design criterion on how to vary the shape factor of nanoparticles in DA arrays in order to obtain the best plasmonic response at a given frequency, and clearly point towards a more robust engineering of DA structures with respect to periodic ones.

5. Summary

In this paper, we have investigated the role of the nanoparticles shape factor in the scattering and localization properties of deterministic aperiodic nanoparticle arrays of metal nanoparticles using a CDA model, which has been validated through a comparison with electromagnetic calculations based on the semi-analytical generalized Mie theory (GMT) and T-matrix theory. Our results have highlighted the advantages of the aperiodic structures by demonstrating stronger field localization and larger values of field enhancement occurring over larger areas with respect to reference periodic structures. In addition, we have investigated engineering design criteria for DA arrays with respect to the arrays morphology and the nanoparticles shape factor, and showed that, contrary to periodic structures, DA arrays can be engineered to simultaneously maximize, at a given wavelength, the far-field scattering efficiency, the electric field enhancement, and the spatial localization of the plasmonic fields. This analysis provides a rigorous framework for the design and engineering of a variety of novel nanoplasmonics devices based on DA arrays, such as reproducible single-molecule SERS substrates, highly sensitive bio-sensors and plasmonic-enhanced non-linear elements.

Acknowledgment

The authors thank Adrian Doicu, Thomas Wriedt, and Yuri Eremin for making their T-matrix Fortran codes available for public use. This work was partially supported by the U.S. Army Research Laboratory under the Contracts No. W911NF-06-2-0040 and No. W911NF-07-1-0618, and the EURATOM/ENEA/CREATE Association.